[19] B. Gold and L. Rabiner, "Parallel processing techniques for estimating pitch periods of speech in the time domain," *J. Acoust. Soc. Amer.*, vol. 46, p. 442, 1969.
[20] E. M. Hofstetter, P. E. Blankenship, M. L. Malpass, and S. Seneff, "Vocoder implementations on the Lincoln digital voice terminal," in *EASCON '77 Rec.*, Sept. 1977.
[21] R. J. McAulay, "Design of a robust maximum likelihood pitch estimator for speech in additive noise," Tech. Note 1979-28, M.I.T. Lincoln Laboratory, Lexington, MA, June 1979.

Robert J. McAulay (S'63-M'67) was born in Toronto, Ont., Canada, on October 23, 1939. He received the B.A.Sc. degree in engineering physics with honors from the University of Toronto in 1962, the M.Sc. degree in electrical engineering from the University of Illinois, Urbana, in 1963, and the Ph.D. degree in electrical engineering from the University of California, Berkeley, in 1967.

In 1967 he joined the Radar Signal Processing Group of the M.I.T. Lincoln Laboratory, Lexington, MA, where he worked on problems in estimation theory and signal/filter design using optimal control techniques. From 1970 to 1975 he was a member of the Air Traffic Control Division at Lincoln Laboratory, and worked on the development of aircraft tracking algorithms, optimal MTI digital signal processing, and on the problems of aircraft direction finding for the Discrete Address Beacon System. On a leave of absence from Lincoln Laboratory during the winter and spring of 1974, he was a Visiting Associate Professor at McGill University, Montreal, P.Q., Canada. Since 1975 he has been a member of the Speech Systems Technology Group at Lincoln Laboratory, where he has been involved in the development of robust narrow-band speech vocoders.

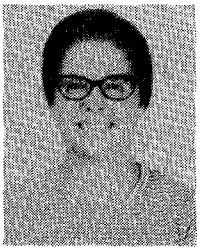

Marilyn L. Malpass was born in Cleveland, OH, on July 18, 1938. She received the B.A. degree in physical sciences and math from Radcliffe College, Cambridge, MA, in 1960.

She joined the M.I.T Lincoln Laboratory, Lexington, MA, as a Programmer in June 1960, and later became a member of the Technical Staff. For the past several years she has been involved in real time speech processing and packet network simulations.

Impact of the Ocean Acoustic Transfer Function on the Coherence of Undersea Propagations

ALBERT A. GERLACH

Abstract—**Multipath propagation, in conjunction with source motion, creates a splitting and spreading of the received source-signal energy over the time register time scale-factor (ambiguity) plane. This splitting of the received signal energy is manifested as correlation interactions between both; the set of eigenray signal arrivals (comprising the multipaths) at each receiving sensor, and the set of eigenray signal correlation pairs comprising two (or more) sensors. The more tightly the sets of eigenray signals are clustered in the ambiguity plane, the stronger will be the signal component interactions at each sensor and the less will be the expected correlation degradation between sensors. However, the greater will be the variance. Conversely, the more diffuse the clustering, the weaker will be the signal component interactions and the greater will be the expected intersensor coherence degradation. Also, the less will be the variance. Criteria which define the degree of signal component interactions in terms of the signal and the ocean transfer function parameters have been defined and are displayed in graphical form.**

Introduction

As a consequence of multipath acoustic propagation, a remotely received signal will consist of the weighted superposition of a number of source signals both slightly compressed (or expanded) and translated in time [1]. The time-variable compression factor is a stochastic process which reflects the fluctuations inherent in both the medium and the source motion. The signal physics are depicted in Fig. 1 for a three eigenray-path model. The diagram is distorted in that the vertical scale is highly exaggerated in comparison with the horizontal scale, and for long ranges (greater than about 200 nmi) the number of path cycles would range from about 7 to greater than 30 (instead of the single cycles shown). The three eigenray paths shown consist of two purely refractive (RR) paths and one refractive surface-reflected (RSR) path. Other paths are also possible [2], [3].

The source signal arriving over each eigenray path differs in relative amplitude A (depicted by the weight of the path), initial time delay τ_0, and time scale-factor shift (or Doppler ratio) δ. For a motional source, the relative amplitudes and the Doppler ratios will be time variable. Signal-wise, the source signal time-scale "t" is transformed into "kt" upon being projected into the medium where $k = 1 + \delta$ is the time scale-factor and δ is the minute scale-factor shift or Doppler ratio. Mathematically, δ is a form of running time average of the scalar or "dot" product between the source velocity and a unit vector along the eigenray path at the source, divided by the sound speed at the source [1]. The Doppler ratios differ as a consequence

Manuscript received January 29, 1979; revised September 6, 1979. This work was supported by the Defense Advanced Research Projects Agency under ARPA Order 3074.

The author is with the Naval Research Laboratory, Washington, DC 20375.

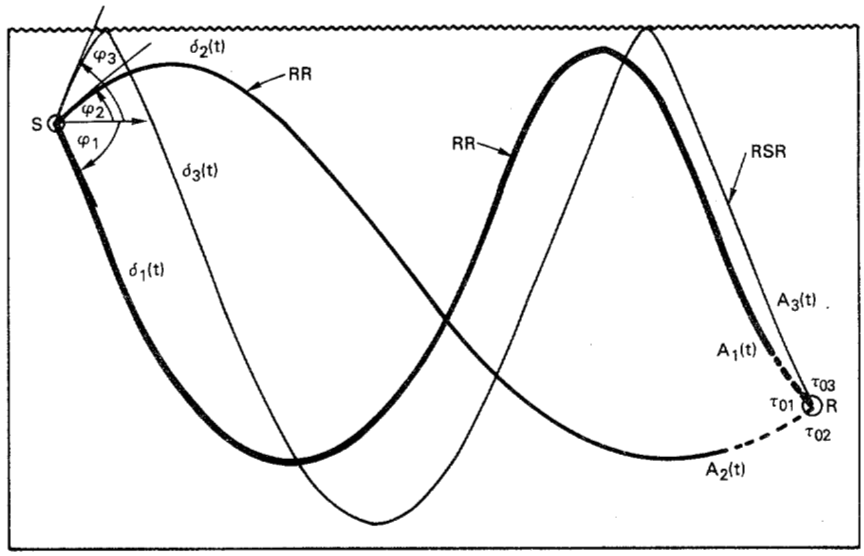

Fig. 1. Ray diagram depicting three eigenray signal propagation paths between a source S and a receiving sensor R. The received signal is the superposition of the source signal arriving over the eigenray paths. Each eigenray signal at R is characterized by an amplitude level A, an initial time delay τ_0, and a time scale-factor shift (or Doppler ratio) δ.

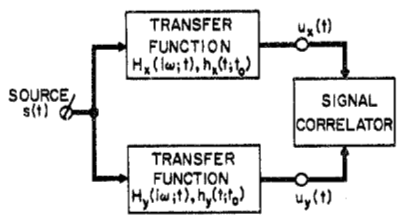

Fig. 2. Communications channel representation of intersensor coherence processing.

of the different eigenray depression (or elevation) angles at the source.

The system under consideration is shown in Fig. 2. The ocean medium (including source motion) is represented as transfer functions between the source and the two receiving sensors. The ocean transfer characteristics modify (or distort) the source signal arriving at the receiving sensors in the manner depicted in Fig. 1. This distortion will be different for widely separated receiving sensors. The impact of this distortion on the coherence between two received signals is the problem being addressed in this paper. A number of approaches covering the many facets of this problem is available in the literature [2]-[9]. This paper will be concerned with determining the expected efficiency of coherent multisensor processing in a deep ocean basin as a function of the signal and medium parameters for a relatively shallow source and deep receiving sensors.

Dual-Path Signal Analyses

Received Signal Relations

Experience has shown that in many instances the number of significant multipaths are reducible to two. For this reason, and for the insight it provides into the signal physics, it is well to study the dual-path situation in some detail. Consider, then, that dual-path narrow-band signals from a moving source are received at two remote receiving sensors. Further, let the received signal at each sensor be preprocessed to equalize the amplitude, time delay, and Doppler shift of the primary (or stronger) eigenray signal at each receiving sensor. The resulting compensated receiving sensor outputs can then be written

$$s_1(t) = u(t) + \alpha_1 u\{k_1(t - \tau_1)\} \tag{1a}$$

and

$$s_2(t) = u(t) + \alpha_2 u\{k_2(t - \tau_2)\} \tag{1b}$$

where

- $u(t)$ is the primary (or stronger) of the narrow-band eigenray signals at each sensor after compensation,
- $\alpha \leqslant 1$ is the ratio of the rms levels of the two eigenray signals after compensation,
- τ is the residual time difference in arrival of the secondary eigenray signal (relative to the primary signal) after compensation,
- $k = 1 + \delta$ is the residual time scale-factor of the secondary eigenray signal after compensation,
- $\delta \ll 1$ is the corresponding time scale-factor shift (or Doppler ratio),

and where the subscript denotes the relevant receiving sensor. (For purposes of this paper, the above equations assume noiseless signal channels.)

A vector diagram of the received dual-path signal is shown in Fig. 3. The primary eigenray signal is the unit vector and the secondary signal is the α vector. The amplitude $A(\omega; t)$ and phase $\theta(\omega; t)$ of the resultant received signal (relative to the primary signal) is the vector sum of the two eigenray signals.

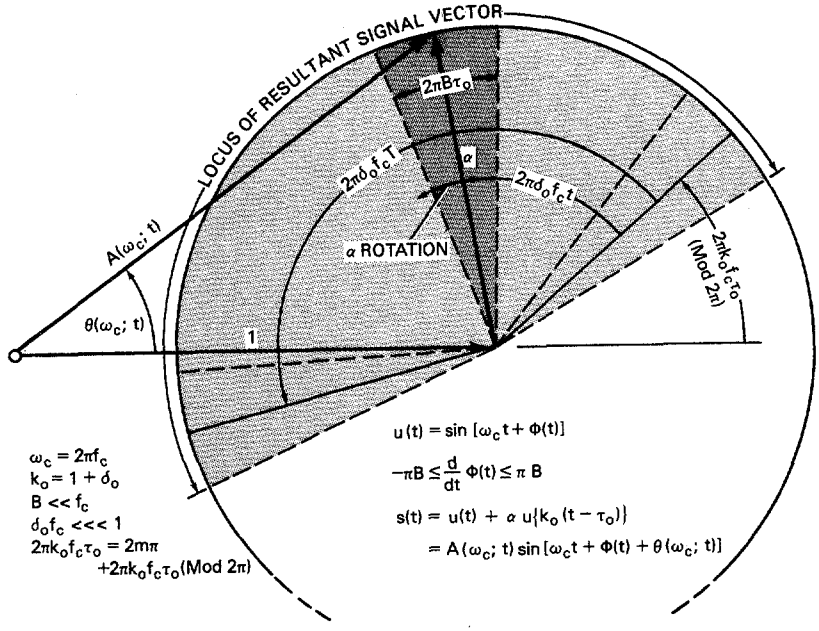

Fig. 3. Vector diagram of a received dual-path signal. (Amplitude parameters are assumed constant over the analysis interval T.)

As a consequence of the residual Doppler difference, the α vector will slowly rotate (from its initial phase position) relative to the unit vector. This is depicted by the lightly shaded area over the observation or analysis interval T. The more heavily shaded area depicts the relative phase modulation resulting from the signal bandwidth B. The diagram illustrates the influence of the signal and transfer function parameters on the resultant received signal characteristics. It should be evident that when the eigenray signal amplitudes vary over the observation time, the resultant vector locus pattern will no longer be circular, but will become somewhat distorted.

Without loss of generality, it will be assumed that the variance or average power of $u(t)$ over the analysis interval is unity. In this circumstance, the variances of the two sensor signals become (averaging over the analysis time T)

$$\sigma_1^2 = \langle s_1^2(t)\rangle = 1 + \alpha_1^2 + 2\alpha_1\gamma(\tau_1; \delta_1) \tag{2a}$$

and

$$\sigma_2^2 = \langle s_2^2(t)\rangle = 1 + \alpha_2^2 + 2\alpha_2\gamma(\tau_2; \delta_2) \tag{2b}$$

where $\gamma(\tau, \delta)$ is the ambiguity function of $u(t)$ (that is, the autocorrelation of the signal over the time-delay and Doppler-shift dimensions). It can be seen that when the secondary signal is widely separated from the primary signal (in the $\tau\delta$ plane), the ambiguity function will be near zero and the average power of the received signal will be essentially $1 + \alpha^2$. This is the case when the received eigenray signals are uncorrelated. On the other hand, when both the time difference and Doppler separation are sufficiently small, the value of the ambiguity function can approach ± 1. In this event, the average received power will vary between approximately $(1 + \alpha)^2$ and $(1 - \alpha)^2$, depending on the phase difference between the received eigenray signals.

The signal physics can be understood from the geometric vector representation illustrated in Fig. 3. When $B\tau_0$ and $\delta_0 f_c T$ are both much less than one (over the analysis interval T), the vector diagram (locus of resulting signal vector) will be more or less static. As a consequence, the power of the received signal (resultant signal vector) will be highly dependent on the mean phase angle of the α vector (secondary signal) relative to the unit vector (primary signal). In this case, the magnitude of the resultant signal vector can range between approximately $1 + \alpha$ and $1 - \alpha$, depending on the relative phase between the eigenray signal vectors. On the other hand, when $B\tau_0$ and/or $\delta_0 f_c T$ is much greater than one, the mean power in the received signal will be the average of the power over all angles about the circle or $1 + \alpha^2$.

Intersensor Correlation Functions

The two-dimensional correlation function between the two sensor channels may be written simply as

$$\begin{aligned}\gamma_{1,2}(\tau, \delta) &= \frac{\langle s_1(kt)\, s_2(t - \tau)\rangle}{\sigma_1\sigma_2} \\ &\approx \frac{1}{\sigma_1\sigma_2}\,[\gamma(\tau, \delta) + \alpha_1\gamma(\tau - \tau_1, \delta + \delta_1) \\ &\quad + \alpha_2\gamma(\tau + \tau_2, \delta - \delta_2) \\ &\quad + \alpha_1\alpha_2\gamma(\tau + \tau_2 - \tau_1, \delta + \delta_1 - \delta_2)]\end{aligned} \tag{3}$$

where the indicated smoothing is computed over the analysis interval T. This relation indicates that four discrete correlation peaks (independent of sidelobes) will occur in the twin dual-path situation, provided the two-dimensional correlation pulsewidth is sufficiently narrow to resolve the peak separations over the $\tau\delta$ (ambiguity) plane.

For narrow-band signals, $\gamma(\tau, \delta)$ will take the form [4]

$$\gamma(\tau, \delta) = \chi(\tau, \delta)\cos\pi\,(2 + \delta)\, f_c\tau \tag{4}$$

where $\chi(\tau, \delta)$ is the two-dimensional correlation envelope (or

coherence) function, $\cos \pi (2+\delta) f_c \tau$ is the carrier function, and f_c is the signal mean frequency. When $(\tau_1 \delta_2 + \tau_2 \delta_1) f_c \ll 1$, it may be shown that the envelope of $\gamma_{1,2}(\tau, \delta)$ (or coherence function) will be

$$\chi_{1,2}(\tau,\delta) \approx \frac{1}{\sigma_1 \sigma_2} [\chi_0^2 + \chi_1^2 + \chi_2^2 + \chi_{21}^2 + 2\chi_0(\chi_1 \cos \pi b_1 + \chi_2 \cos \pi b_2 + \chi_{21} \cos \pi b_3) + 2(\chi_1 \chi_2 \cos \pi b_4 + \chi_1 \chi_{21} \cos \pi b_2 + \chi_2 \chi_{21} \cos \pi b_1)]^{1/2} \quad (5)$$

where

$$\chi_0 = \chi(\tau, \delta)$$
$$\chi_1 = \alpha_1 \chi(\tau - \tau_1, \delta + \delta_1)$$
$$\chi_2 = \alpha_2 \chi(\tau + \tau_2, \delta - \delta_2)$$
$$\chi_{21} = \alpha_1 \alpha_2 \chi(\tau + \tau_2 - \tau_1, \delta + \delta_1 - \delta_2)$$
$$b_1 = 2 f_c' \tau_1' \pmod 2$$
$$b_2 = 2 f_c' \tau_2' \pmod 2$$
$$b_3 = b_2 - b_1$$
$$b_4 = b_2 + b_1$$
$$f_c' = (1 + \delta/2) f_c$$
$$\tau_1' = \tau_1 - (\delta_1/2)(\tau - \tau_1)$$
$$\tau_2' = \tau_2 - (\delta_2/2)(\tau + \tau_2).$$

The first four terms in (5) are the coherence functions of the independent pairwise eigenray signals between the two channels. The remaining six terms express the coherence interaction between the correlation pairs. When the peaks of the independent correlation pairs are sufficiently separated over the ambiguity plane, the interaction terms will be negligible. Otherwise, the coherence topology of the sensor signals will depend on the relative phase between the received eigenray signals (b parameters).

The preceding relations are considerably simplified when only one of the two sensor channels includes a significant secondary eigenray path (that is, when either α_1 or α_2 is zero). Letting $\alpha_2 = 0$, (3) reduces to

$$\gamma_{1,2}(\tau,\delta) = \frac{1}{\sigma} [\gamma(\tau,\delta) + \alpha\gamma(\tau - \tau_0, \delta + \delta_0)] \quad (6a)$$

where $\sigma = \sigma_1$, $\alpha = \alpha_1$, $\tau_0 = \tau_1$, and $\delta_0 = \delta_1$. The corresponding coherence function reduces to

$$\chi_{1,2}(\tau,\delta) = \frac{1}{\sigma} [\chi^2(\tau,\delta) + \alpha^2 \chi^2(\tau - \tau_0, \delta + \delta_0) + 2\alpha\chi(\tau,\delta)\chi(\tau - \tau_0, \delta + \delta_0) \cos \pi b]^{1/2} \quad (6b)$$

where $b = 2 f_c' [\tau_0 - (\delta_0/2)(\tau - \tau_0)] \pmod 2$. In this event, one can expect a twin correlation peak (ignoring sidelobes) when either or both τ_0 and δ_0 are sufficiently large to resolve the correlation peaks separately.

Envelope Partitioning Over the Ambiguity Plane

To study the effect of the system parameters on the intersensor coherence topology, it will be necessary to specify the correlation envelope function $\chi(\tau, \delta)$. Unfortunately, the envelope ambiguity function will depend on the specific source signal employed. However, in the neighborhood of the coherence peak, and for a random narrow-band signal of information bandwidth B and mean frequency f_c, a suitable approximation of $\chi(\tau, \delta)$ is given by [10]

$$\chi(\tau,\delta) = \frac{\sin \pi\delta f_c T}{\pi\delta f_c T} \frac{\sin \pi B\tau}{\pi B\tau}. \quad (7)$$

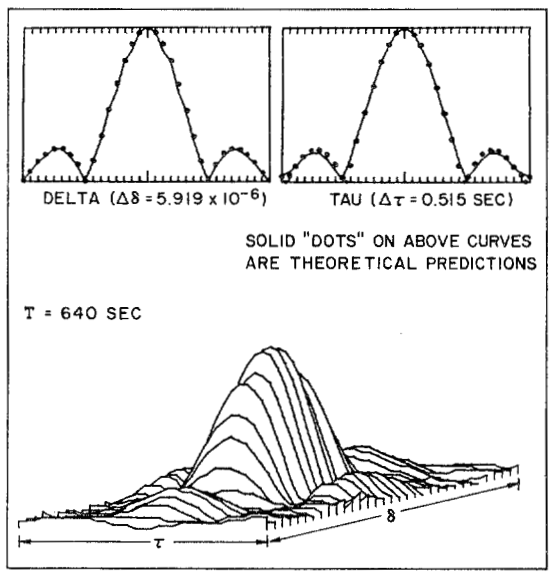

Fig. 4. Envelope ambiguity function for a pseudorandom signal of bandwidth 0.25 Hz and mean frequency 33 Hz. (Note: in the diagram, $\Delta\tau \simeq 1/8B$ and $\Delta\delta \simeq 1/8 f_c T$ define the measures between "tic" increments on the two correlogram cuts through the coherence peak.)

That this is a suitable representation of the envelope ambiguity function is demonstrated in Fig. 4. This is the measured ambiguity function for a pseudorandom frequency-modulated source signal of center frequency 33 Hz and information bandwidth 0.25 Hz. The analysis time was 640 s. (The upper two curves are cuts through the correlation peak along the τ and δ axes, respectively.) The theoretically computed points on the two upper curves were obtained using (7).

The envelope ambiguity function as a function of the relevant system parameters can be computed from (6b) using (7). The effect on the coherence function topology will be demonstrated varying the three parameters τ_0, δ_0, and b in selected sequence. In Fig. 5, the parameters b, α, and $2B\tau_0$ have been fixed at 1, 0.95, and 0.50, respectively, and the parameter $2\delta_0 f_c T$ was varied in steps over the range of 0-2.00. (For convenience, the symbols $\Delta\tau$ and $\Delta\delta$ are used to define the values $1/2B$ and $1/2 f_c T$, respectively. They represent the Nyquist-equivalent bounds on the incremental sampling of the two ambiguity function variables.) The value of $b = 1$ implies that the two eigenray signals arrive essentially 180° out of phase (see Fig. 3). The arrows along the axes of the two correlogram cuts (in each diagram of Fig. 5) show the location of the secondary eigenray signal in the ambiguity plane. (The location of the primary signal will always be 0, 0.) In the sequence of diagrams, the value of $\delta_0/\Delta\delta$ is varied from values below $\tau_0/\Delta\tau$ to values greater than $\tau_0/\Delta\tau$.

Two significant aspects of the coherence topology are to be noted. First, it is seen that the separation of the two prominent topological peaks is essentially constant and well in ex-

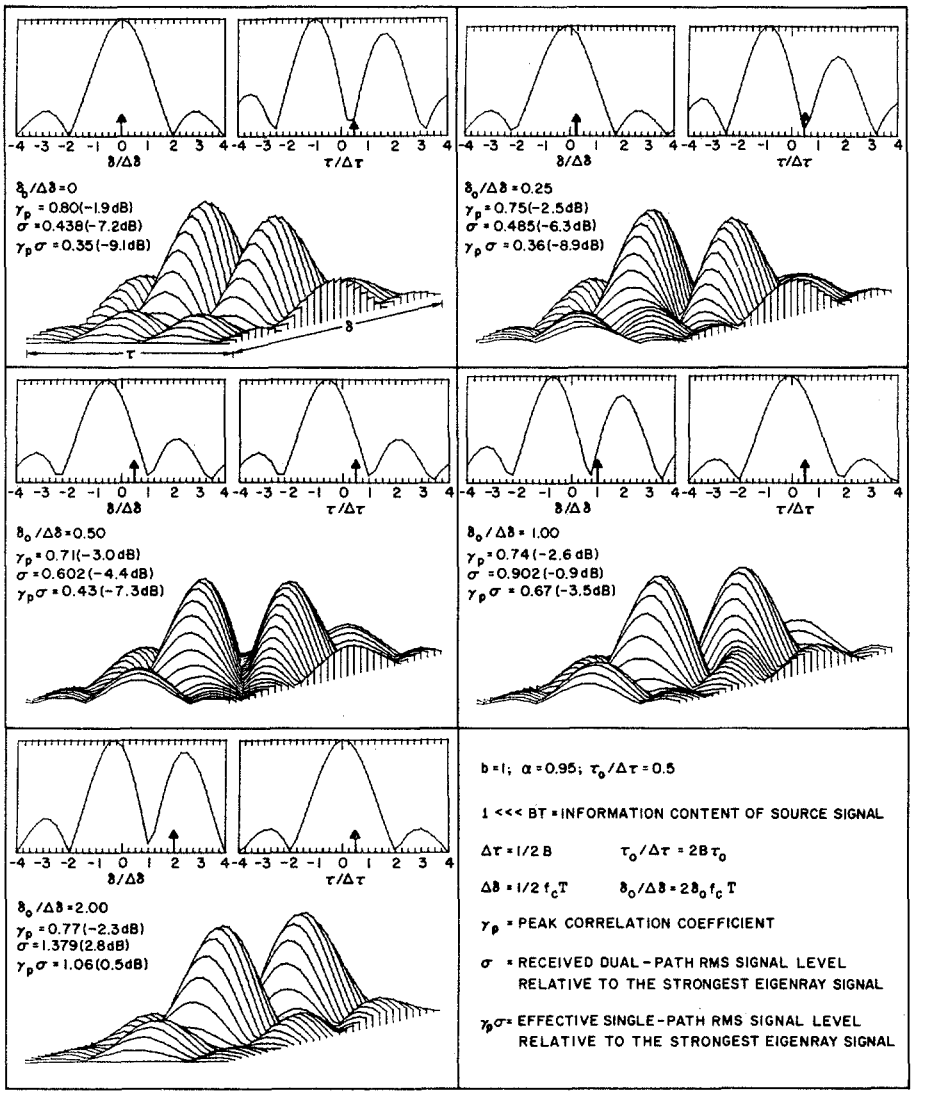

Fig. 5. Correlation envelope topology, resulting from a dual-path channel, showing the effect of the relative locations of the primary and secondary eigenray signals (in the ambiguity plane) on the partitioned envelope geometry. Arrows along the abscissa of the τ and δ cuts (located above each correlogram) show the location at the secondary signal. The primary signal is located at 0, 0 in each case.

cess of the separation of the two eigenray signal locations in the ambiguity plane. The peaks are also nearly symmetrically spread about the locations 0, 0 and $\tau_0/\Delta\tau$, $\delta_0/\Delta\delta$. This phenomenon we have chosen to call "envelope partitioning in the ambiguity plane." It occurs whenever τ_0 and δ_0 are both less than about $2\Delta\tau$ and $2\Delta\delta$, respectively, and the parameter b is close to unity. The second thing to note is that the secondary peak rotates about the primary peak as the magnitude of $\delta_0/\Delta\delta$ approaches and then exceeds the magnitude of $\tau_0/\Delta\tau$. When these two parameters are equal, the location of the two peaks lie along a 45° line over the normalized ambiguity plane.

Data given on each diagram include the peak correlation coefficient γ_p, the rms signal level of the dual-path channel σ, and the value $\gamma_p\sigma$. This last value is the effective rms level of the dual-path channel from a detection standpoint. (That is, it represents the rms level of an ideal single-path channel which would produce the same peak coherence output as the given dual-path channel.) Thus, when $\gamma_p\sigma$ is less than one, the presence of the secondary eigenray signal is destructive to correlation processing. On the other hand, when $\gamma_p\sigma$ is greater than one, the presence of the secondary signal enhances correlation processing. In the case of Fig. 5, the presence of the secondary signal path is destructive to correlation processing until $\delta_0/\Delta\delta$ equals or exceeds about 2. For very large values of $\delta_0/\Delta\delta$, the value of $\gamma_p\sigma$ approaches unity.

In Fig. 6, the parameters b and α are again fixed at 1 and 0.95, respectively. The parameters $\tau_0/\Delta\tau$ and $\delta_0/\Delta\delta$ are set equal and varied in steps over the range of 0.25-3.00. It may be noticed that the topology remains relatively invariant until the values of the two parameters exceed about 1.89. Beyond this critical point, the secondary coherence peak separates from the partitioned-envelope state and becomes relatively independent of the primary coherence peak. More generally, breakaway from the partitioned-envelope state occurs when the root mean square of the parameters $\tau_0/\Delta\tau$ and $\delta_0/\Delta\delta$ exceeds approximately 8/3. Below this critical value, the separation of the two primary peaks in the normalized (illustrated) ambiguity plane is approximately equal to 8/3. Beyond this

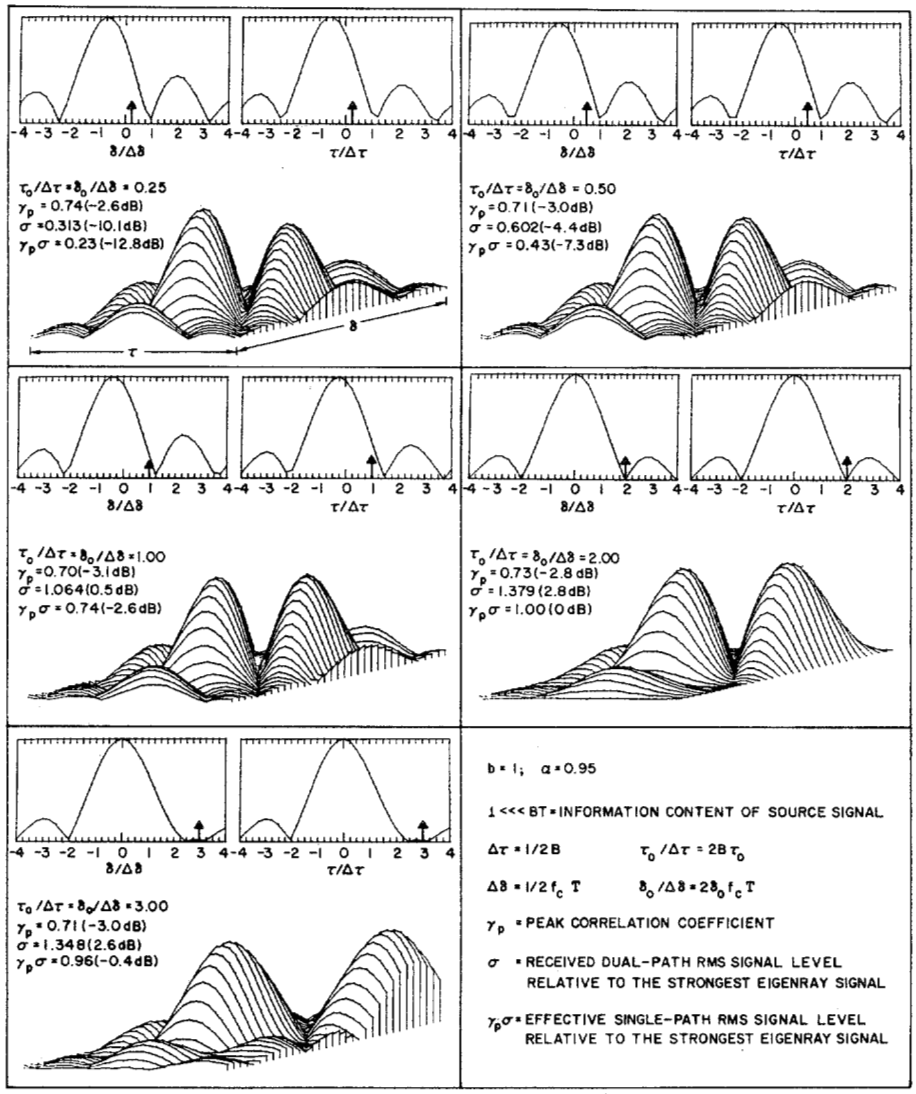

Fig. 6. Correlation envelope topology, resulting from a dual-path channel, showing the effect of the separation of the primary and secondary eigenray signals (in the ambiguity plane) on the twin envelope peaks. Arrows along the abscissa of the τ and δ cuts (located above each correlogram) show the location of the secondary signal. The primary signal is located at 0, 0 in each case.

critical point, the two eigenray correlation pairs are only weakly interactive, and the detection sensitivity of the correlation processor approaches that which would be realized from the presence of the strongest of the two eigenray signals alone. The presence of the secondary signal then serves merely to spread the coherence topology over the ambiguity plane.

A study of the parameter tabulations on each diagram in Fig. 6 reveals that the detection sensitivity of the dual-path channel increases with increased values of the parameters out to the point where these values are approximately 2. Beyond this point, there occurs a minor cyclical undulation of $\gamma_p \sigma$ which asymptotically decays to unity for large values of the parameters.

In the correlograms presented up to this point, the presence of the secondary eigenray signal has proven generally destructive to the cause of correlation processing. This is a result of the fact that the parameter b was chosen as precisely unity, which dictates that the frequencies of the dual-path signals be effectively 180° out of phase (see Fig. 3). In this situation, increasing the separation of the eigenray signals in the ambiguity plane generally improved the detection sensitivity of the correlation process (reduced the destructive effect of the secondary eigenray signal). It will now be well to examine the effect of the parameter b on the coherence topology when the other parameters are held fixed.

In Fig. 7, the parameter α is fixed at 0.95, and $\tau_0/\Delta\tau$ and $\delta_0/\Delta\delta$ are both fixed at 0.50. In this set of diagrams, the parameter b is varied in steps from 1 to ±0.50 (corresponding to a phase difference between 180 and ±90°). It will be noticed that as b deviates from 1, the envelope partitioning effect rapidly decays until only a single peak occurs for b less than or equal to about 0.8. Moreover, since b can be considered a random variable with uniform probability density over the range ±1, it can be concluded that envelope partitioning will be evident over less than 20 percent of the time. As the absolute value of b is reduced from 0.8 to 0, the sharpness of the result-

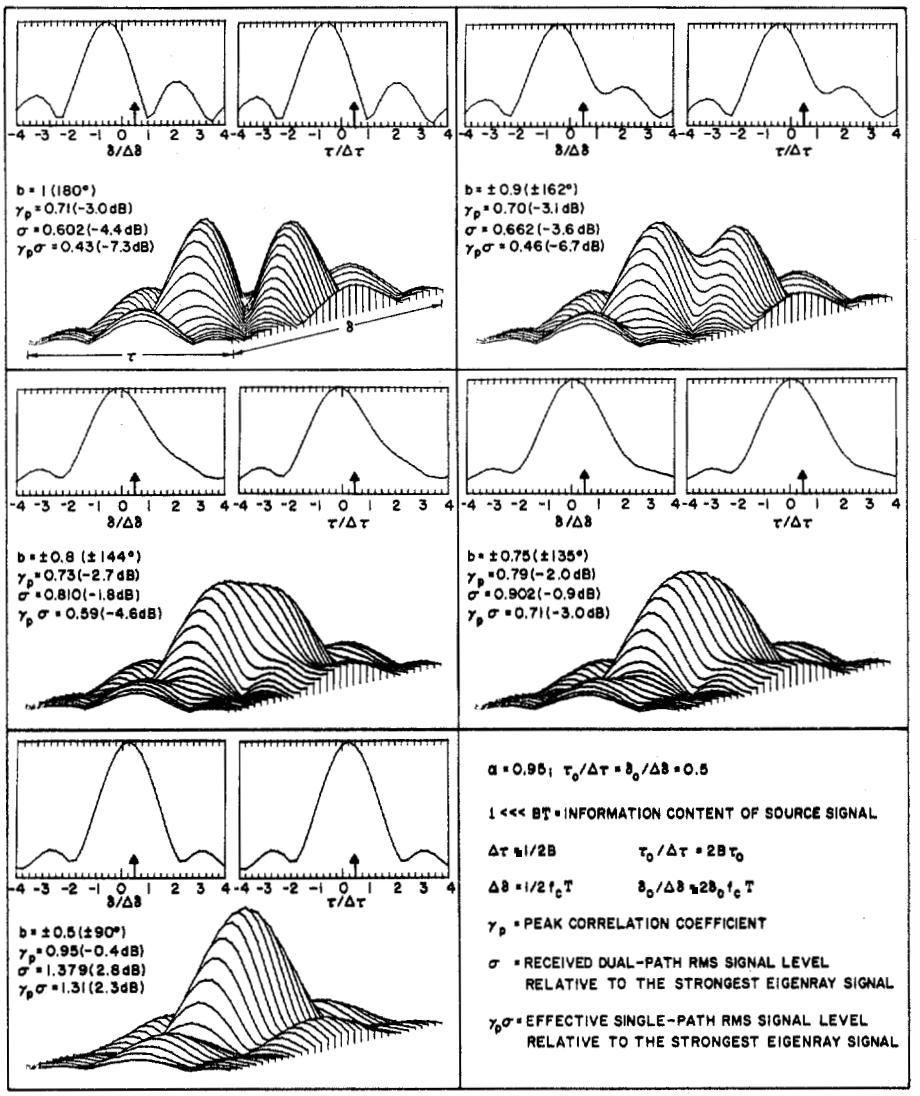

Fig. 7. Correlation envelope topology, resulting from a dual-path channel, showing the influence of the phase parameter b in producing the partitioned envelope state. Arrows along the abscissa of the τ and δ cuts (located above each correlogram) show the location of the secondary eigenray signal. The primary eigenray signal is located at 0, 0 in each case.

ing single peak, as well as the peak correlation coefficient and average received power, will increase. The system becomes optimum when b equals zero.

It may further be noted that whereas the secondary eigenray signal is generally destructive to the cause of correlation processing for b in the neighborhood of 1, the secondary path will enhance correlation detection over the greater portion of the permissible range of b. However, the peak signal degradation exceeds the peak signal enhancement to at least partially offset the greater range of b over which enhancement occurs. For the example shown (Fig. 7), enhancement occurs over about 63 percent of the range of b, while degradation occurs over only 37 percent of the range. On the other hand, the maximum coherence enhancement is 5.39 dB, while the maximum degradation is -7.33 dB. The average over all b is in favor of enhancement by about 1.7 dB. Overall it appears that secondary eigenray signal paths enhance (in a statistical sense) the peak correlation over that realized by the primary paths alone. However, the presence of the secondary signals can markedly increase the variance of the intersensor peak coherence (and thus the target detectability) over time.

Calculation of the Time Scale-Factor Shift Parameter

It is of interest to determine the amount of time scale-factor shift (or Doppler ratio) that can be expected between eigenray signals in practical applications. This will determine the degree of peak coherence separation over the ambiguity plane which can be expected from the set of intersensor eigenray correlation pairs.

It has been shown that the expected time scale-factor shift for a signal projected into the propagation medium (Fig. 1) is essentially the scalar or dot product of the source velocity and a unit vector along the eigenray path of the source divided by the sound propagation speed at the source [1]. Therefore, the expected difference between the time scale-factor shifts of two eigenray signals can be written simply as

$$\delta_{mn} = \frac{\dot{R}}{c}(\cos\varphi_m - \cos\varphi_n) \tag{8a}$$

where $\dot{R}$ is the effective range rate of the source to the receiving sensor, c is the sound speed at the source, and φ_m and φ_n are the depression (or elevation) angles of the relevant eigenray paths at the source (Fig. 1). For long-range signal propagation, the magnitudes of the significant eigenray depression angles will be small (generally less than 15°), so (8a) can be approximated as

$$\begin{aligned}\delta_{mn} &\approx 5.29R(\varphi_n^2 - \varphi_m^2) \times 10^{-8} \\ &= 1.058\dot{R}\bar{\varphi}_{nm}\Delta\varphi_{nm} \times 10^{-7}\end{aligned} \tag{8b}$$

where

$\dot{R}$	is the effective range rate in knots,
φ_m and φ_n	are the relevant eigenray depression angles in degrees,
$\bar{\varphi}_{nm}$	is the mean of the two depression angles in degrees,
$\Delta\varphi_{nm}$	is equal to the difference $\varphi_n - \varphi_m$ in degrees,

and a sound propagation speed of 2880 knots is assumed. The frequency difference between the two eigenray signals is essentially $\delta_{mn}f_c$. Consequently, eigenray signal frequency differences of only a very small fraction of a hertz can be expected in practical applications. The phase migration between the relevant eigenray signals over the analysis interval will be essentially $2\pi\delta_{mn}f_cT$ (see Fig. 3).

General Multipath Analyses

In the preceding analyses, only a single dual-path channel was used to demonstrate the influence of the system parameters on the resulting intersensor coherence topology. When both signal channels comprise dual-path signals, the complexity of the analysis is increased appreciably due to the additional transfer function parameters which must be taken into consideration. And when one considers greater than two paths for the sensor channels, the problem becomes prohibitive to analyze in detail. However, by utilizing the source signal parameters to normalize the scales of the ambiguity plane, and by representing both the received sensor signals and the resulting intersensor coherence function as vector sets, some very useful conclusions can be formulated for the general multipath propagation case. In the analyses to follow, a rather comprehensive insight will be obtained of how both the signal and the transfer function parameters determine the effectiveness of correlation processing in practical applications.

Eigenray Vector Sets

A study of Fig. 1 reveals that the ocean transfer function is characterized by the set of parameters $A_i(t)$, τ_{0i}, and $\delta_i(t)$ where $i = 1, 2, \cdots, m$ denotes the eigenray paths of significance over some analysis interval T. In addition, a narrowband signal source can typically be characterized by a mean frequency f_c and an information bandwidth B over the analysis interval T. For convenience, new variables ξ and η are defined as

$$\xi \equiv B\tau \quad \text{and} \quad \eta \equiv f_cT\delta, \tag{9}$$

normalizing the ambiguity function variables τ and δ. This will have the effect of merging the signal parameters with the medium parameters. Under these circumstances, the signals at the two receiving sensors (Fig. 2) can be represented as sets of triads or eigenray vectors which comprise the received signals. Thus, over the relevant analysis interval T

$$u_x(t) \rightarrow \{A_{xi}(t); \xi_{xi}, \eta_{xi}(t)\}_m \qquad (i = 1, 2, \cdots, m) \tag{10a}$$

and

$$u_y(t) \rightarrow \{A_{yj}(t); \xi_{yj}, \eta_{yj}(t)\}_n \qquad (j = 1, 2, \cdots, n) \tag{10b}$$

where $u_x(t)$ and $u_y(t)$ are comprised of m and n eigenray signals, respectively, and

$$\xi_{xi} \equiv B\tau_{oxi}, \eta_{xi}(t) \equiv f_cT\delta_{xi}(t), \text{ etc.} \tag{10c}$$

The above vector representation of the received signals is shown schematically in Fig. 8. The eigenray signal amplitudes are displayed by the height above the $\xi\eta$ plane, and the locations are distributed over the plane. Due to the time variable nature of the eigenray signals, the vectors may wander (or fluctuate) along the A and η dimensions over the observation time T. This wandering is due both to the source motion and the medium fluctuations; however, the effects of the latter are generally small compared with the effects of the former.

Intraset Correlation

To assess the correlation interaction between members of a given set, a unit circle is drawn around the location of each eigenray vector in the $\xi\eta$ plane (Fig. 8). Where the unit circles for particular vector locations do not overlap other circles, the intracorrelation of these members with the other members of the set will be negligible. The energy from these signals will add directly in determining the total energy (or average power) of the received signal. Where particular circles overlap but do not enclose each other's origins, the expected intraset correlation will be low to moderate. However, where particular circles overlap sufficiently to enclose each other's origins, the expected intraset correlation between the relevant members can be moderate to high. The exact correlation between the relevant members in these latter two cases will depend on both the degree of unit circle overlap and the relative phase between the signals at the receiving sensor. The contribution to the received signal energy in these latter two cases will depend on the amplitudes of the relevant eigenray signals as well as the intraset correlation coefficient. In the example illustration (Fig. 8), none of the unit circles overlaps. In this event, the received signal energy from each sensor channel is simply the sum of the energy in each of the eigenray signals comprising the set. Should all (or several) of the unit circles overlap, the expected received energy would exceed this sum. However, the variance would be such that greater or less than this sum could be realized.

Correlation-Pair Set

From Fig. 8, one can perceive that two-dimensional cross correlation of the two sensor channels results in the superposi-

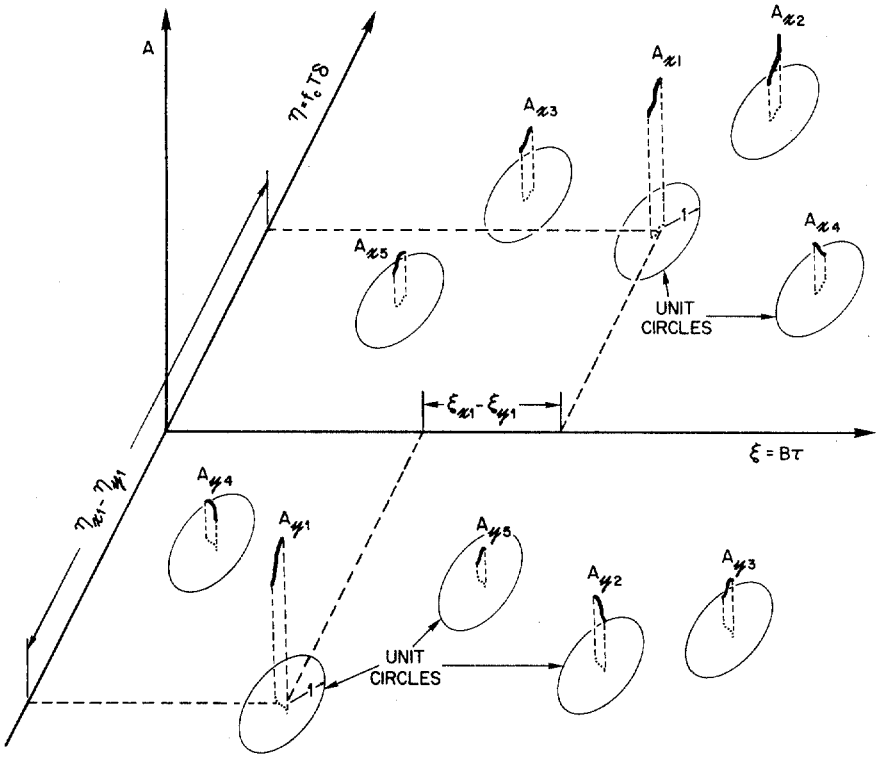

Fig. 8. Schematic representation of two sensor-channel eigenray vector sets in the $A\xi\eta$ space. Splitting and spreading of the arriving signal energy over the ambiguity plane are demonstrated. Unit circles define the boundaries of intraeigenray-signal correlation for each channel.

tion of m times n cross-correlated eigenray signal pairs where the correlation peaks of the discrete pairs are distributed over the ambiguity plane. Consequently, it will prove convenient to represent the two-dimensional cross correlation of the sensor channels as the vector set

$$\gamma_{x,y}(\tau,\delta) \rightarrow \{\gamma_{pk};\xi_k,\eta_k\}_{mn} \quad (k=1,2,\cdots,mn) \quad (11a)$$

where the vector components are the magnitude and location of the peak coherence for the mn discrete correlation pairs considered individually. The relationship to the eigenray vector components is

$$\{\gamma_{pk};\xi_k,\eta_k\} \sim \{F_{i,j}(A_{xi}A_{yj});\xi_{xi}-\xi_{yj},\eta_{yj}-\eta_{xi}\}. \quad (11b)$$

The above relation implies that the pairwise coherence peaks will occur at the locations $\xi_{xi}-\xi_{yj}$, $\eta_{yj}-\eta_{xi}$ over the ambiguity plane, and the magnitude of the peak coherence will be a function of the product of the relevant eigenray signal amplitudes. For stationary eigenray vectors, the magnitude of the peak coherence will be directly proportional to the product of the relevant signal amplitudes. However, due primarily to source motional characteristics, coherence degradation can be expected for the individual correlation pairs [11]. Thus, a simple formulation of the magnitude of the pairwise peak coherence is not possible in the general case. In any event, the concept of the discrete eigenray correlation-pair set is an extremely useful one, as will be demonstrated shortly.

Intersensor Correlation

To assess the intersensor correlation, a unit circle may be drawn around each correlation-pair location in the ambiguity plane as shown in Fig. 9. Where the circle for a given correlation pair does not overlap any of the circles from the remaining correlation pairs, the coherence of the relevant pair will be essentially independent of the other signals and may be treated separately. The effect of this correlation on the remaining correlations will also be insignificant. Where two or more circles overlap but do not enclose each other's origins, the expected correlation interaction between the relevant pairs will be weak to moderate. On the other hand, where two or more unit circles overlap sufficiently to enclose each other's origins, the expected correlation interaction will be moderate to strong,

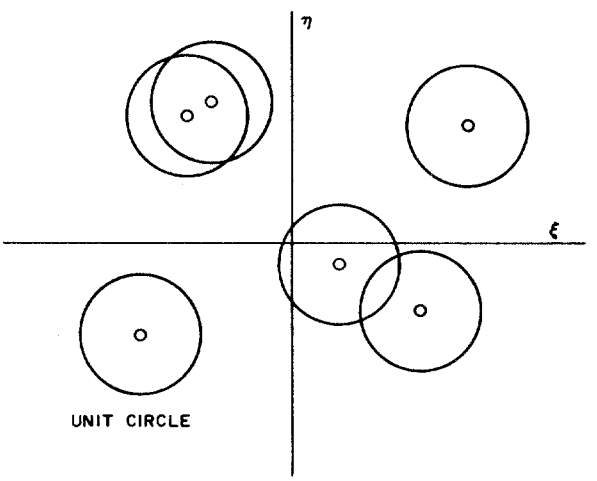

Fig. 9. Correlation-pair vector locations in the $\xi\eta$ plane. Unit circles define the boundaries of correlation interaction between members of the set. Three degrees of correlation-pair interaction are demonstrated by the relative overlap of the unit circles.

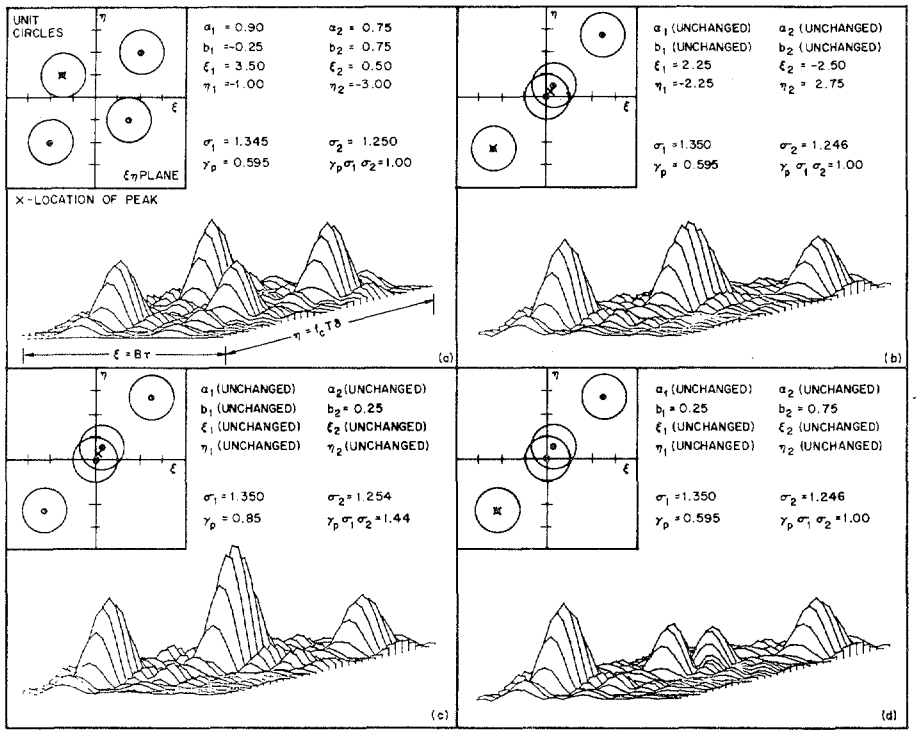

Fig. 10. Twin dual-path signal correlograms showing the effect of the correlation-pair locations and eigenray signal phases on the resultant topology. In each case, the dual-path eigenray signals are essentially uncorrelated. The locations of the independent pairwise correlation peaks (as well as the location of the resultant coherence peak) are shown in the plan-view $\xi\eta$ plane.

permitting a wide variety of coherence topologies to occur in their immediate neighborhood. The resulting intersensor coherence topology will depend on the number and degree of unit circle overlap, and on the relative amplitudes and phases of the relevant eigenray signals at the two receiving sensors.

Examples

To demonstrate the principles expounded above, (5) was used to compute the coherence topology for two dual-path signal channels. In all of the examples to be presented, the ocean transfer function parameters will be assumed stationary over the relevant analysis interval. The amplitude ratios of the secondary-to-primary eigenray signals for the two channels are set to 0.90 and 0.75, respectively. The relative locations and phases of the eigenray signal pairs will be varied (in ordered sequence) to demonstrate their effect on the resulting intersensor coherence topology.

In the first set of examples, the separation of the eigenray signal vectors (in the ambiguity plane) is made sufficiently large so that the unit circles do not overlap. In this situation, the received signal power will remain essentially unchanged in these examples. The results from four examples are shown in Fig. 10. Each illustration displays a listing of the assigned and computed parameters, the resulting coherence topology, and a plan view of the normalized ambiguity plane showing the locations of the eigenray correlation-pair set. The "b" parameters are a measure of the phase difference between the dual-path eigenray signals in each channel [see (5)], and can range over ± 1. The σ's are the received rms levels of each channel, and γ_p is the resultant peak coherence (or correlation coefficient) between channels. The parameter $\gamma_p \sigma_1 \sigma_2$ is the equivalent single-path cross power which would give the same peak correlation as the twin dual-path channels. When this value is 1, the equivalent single-path channels are simply the two primary eigenray signals. When this value is less than 1, the presence of the secondary signals actually degrades the correlation of the primary eigenray signals alone. When this value is greater than 1, the secondary eigenray signals enhance the correlation of the primary signals.

In Fig. 10(a), none of the unit circles overlaps, so the resulting intersensor coherence is simply the sum of the coherence for the eigenray correlation pairs taken singly. The correlation interaction terms [see (5)] are essentially zero, so that varying the phase parameters will have a negligible effect on the resulting coherence topology. In this case, the peak of the resulting correlogram occurs at the peak of the correlation pair comprising the two primary eigenray signals. (In the example, this is located in the second quadrant of the ambiguity plane, as shown.) Although specific values are given for the two phase parameters (b_1 and b_2), the resulting coherence topology is essentially independent of these parameters.

In the remaining three examples of Fig. 10, the locations of the eigenray signal vectors are fixed and only the phase parameters are varied. It will be observed that only in the neighborhood of the overlapping unit circles is the coherence topology affected. And only in Fig. 10(c) is the resultant peak coher-

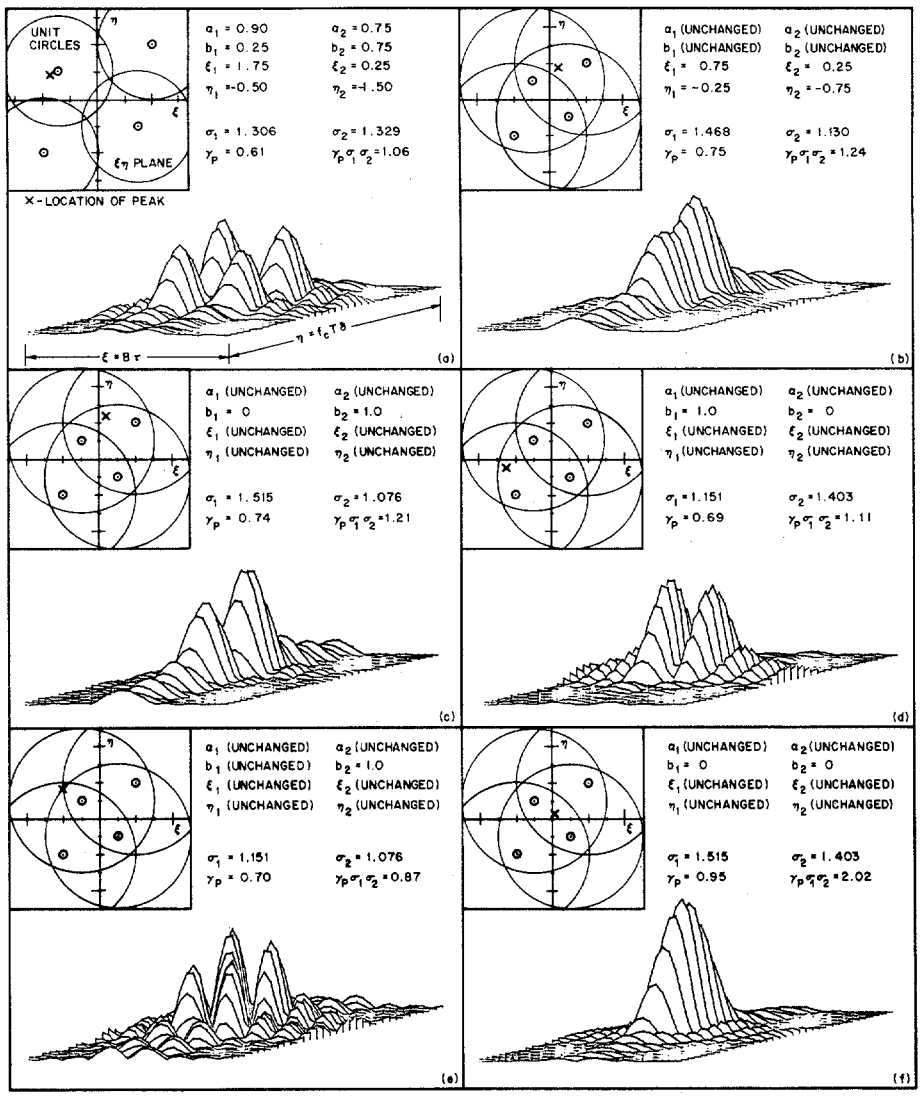

Fig. 11. Twin dual-path signal correlograms (as in Fig. 10) for the case where the dual-path eigenray signals are correlated. The influence of the dual-path signal phase parameters (b_1 and b_2) becomes highly significant when the unit circles enclose each other's origins.

ence enhanced over that of the two primary eigenray signals alone. (In these examples, the peak coherence of the two primary eigenray signals lies in the third quadrant of the ambiguity plane.) Thus, when the eigenray signals of the two sensor channels are all uncorrelated, the peak coherence of the two channels is no worse (and generally no better) than the peak coherence of the primary eigenray signals alone.

In the second set of examples, the separation of the dual-path signals in the ambiguity plane has been decreased so that the unit circles about the eigenray vectors overlap. In this situation, nonnegligible correlation can exist between the eigenray pairs, and interaction between correlation pairs can be anticipated. Six examples showing the resulting coherence topologies are shown in Fig. 11. In Fig. 11(a) the unit circles about both the eigenray vectors and the correlation-pair vectors overlap only slightly. In this event, the expected intra- and intercorrelation interaction will be weak to moderate, producing only modest changes in the coherence topology with variations in the phase parameters. It may be noticed that the location of the resultant peak coherence is slightly removed from the location of the peak coherence of the pairwise primary eigenray signals alone (second quadrant of the ambiguity plane).

In the remaining five examples, the separation of the eigenray vectors has been reduced to the point where the unit circles enclose each other's origins. In these examples, the locations of the eigenray vectors are held fixed, and the phase parameters alone are varied. A study of Fig. 11(b)-(f) reveals the wide variety of coherence topologies (including envelope partitioning) realizable with changes in the two eigenray phase parameters. Of significance also is the corresponding variation in both the magnitude and the location (in the ambiguity plane) of the resultant peak coherence. All of these variations are manifested as fluctuations, in real-world applications, since the phase parameters are truly random in character. In this strong correlation interaction situation it is evident that the

expected peak coherence is enhanced by the presence of the secondary eigenray signals; however, the variance is also quite high.

Correlation Interaction Zones

In the previous analysis, the unit circle in the ambiguity plane provided a direct and graphic measure of the degree of interaction to be anticipated between members of the eigenray and correlation-pair vector sets. It will be of interest, therefore, to transform the unit circle criteria into boundaries which can be interpreted in terms of the relevant system parameters. To accomplish this, it will be recalled (see Fig. 8) that the separation between eigenray vectors along the ξ and η dimensions are, respectively,

$$|\xi_m - \xi_n| = B\,|\tau_{om} - \tau_{on}| \tag{12a}$$

and [using (8b)]

$$|\eta_m - \eta_n| = f_c T\,|\delta_m - \delta_n| = 1.058\, f_c T\,|\dot{R}\bar{\varphi}_{nm}\Delta\varphi_{nm}| \times 10^{-7} \tag{12b}$$

where the subscripts m and n denote two arbitrary members of the eigenray vector set. The separation between correlation-pair vectors is a little more complicated, but should follow the same statistical trend as the eigenray vectors. That is, where the eigenray vector sets of the two sensors are tightly clustered, the corresponding correlation-pair set will be equally tightly clustered. On the other hand, where the eigenray vector sets are widely dispersed, the corresponding correlation-pair set will also be widely dispersed. The latter set, however, may comprise many more members than either of the former, so that limited subset clustering can occur in the correlation-pair set even when the eigenray vector sets are widely dispersed. [This is what occurred in the example shown in Fig. 10(b)-(d).] In any event, the separation of the eigenray vectors provides a useful measure of the coherence interaction to be expected in practical applications.

In the real ocean environment, both the time delay and the depression angle differences are functions of many variables (range, source and receiving sensor depths, sound speed profiles, etc.). And the ensemble of probable values for each of these differences would provide a basis for their distribution functions. If sufficient data were available, one could determine the distribution functions for the variables $|\tau_{om} - \tau_{on}|$ and $|\bar{\varphi}_{nm}\Delta\varphi_{nm}|$, and select suitable upper and lower bounds for these variables. Unfortunately, an accurate description of the relevant distribution functions is not known, so a purely intuitive estimate of roughly the 10 and 90 percent probability bounds on these variables will be made by the author.

In the case of the propagation delay, the temporal extent of the significant multipath arrivals appears to be proportional to the propagation range for ranges greater than about 100 nmi. This is not necessarily a smooth linear function, but simply a general trend. Within the SOFAR channel, the temporal distribution of the multipaths is smooth and amounts to about 1 s/100 nmi of transmission range [12]. However, for a source and/or receiving sensor located remote from the sound channel axis, the temporal distribution of the received eigenray signals can be rather erratic [13]. Also, the temporal extent of the significant multipaths is not a smooth function of range, and is generally less than about 2 s/100 nmi of transmission range. Based upon limited observations, suitable bounds for the eigenray separation in the ξ dimension are estimated as

$$BR/2000 \leqslant |\xi_m - \xi_n| \leqslant BR/200 \tag{13a}$$

where R is the source-to-sensor range in nautical miles and B is the information bandwidth of the signal in hertz.

In the case of the Doppler ratio difference, the extent of the significant depression angles is generally less than about $\pm 15°$. Consequently, suitable bounds for the eigenray separation in the η dimension are estimated as

$$f_c T\dot{R}/30\,000 \leqslant |\eta_m - \eta_n| \leqslant f_c T\dot{R}/3000 \tag{13b}$$

where $\dot{R}$ is the source range rate in knots, f_c is the mean signal frequency in hertz, and T is the analysis time in minutes.

Although somewhat arbitrary, these bounds can be used to interpret the unit circle criteria in terms of the relevant system parameters for long-range propagation. The bounds given by (13) are displayed graphically in Fig. 12. This zonal map illustrates the statistical implications of the unit circle criteria in terms of parameters more readily assimilated by the applications engineer. The map is partitioned into three interaction zones, with shading depicting the relative degree of expected correlation interaction over the area. The strong interaction zone represents the area where the ensemble of eigenray and correlation-pair vectors generally fall within each other's unit circles. The weak interaction zone represents the area where unit circles about the ensemble of eigenray and correlation-pair vectors generally do not overlap. The transition zone represents the area where a mixed situation is likely to occur. The dimensions of the two scales are interesting in that the ordinate is the product of the mean signal frequency and the change in range over the analysis interval, while the abscissa is the product of the range and the change in the signal frequency (bandwidth) over the analysis interval. The magnitudes of these two factors determine the efficiency of intersensor coherence processing in practical applications.

Conclusions

Multipath propagation is manifested as a splitting and spreading of the eigenray signal energy over the ambiguity plane. Due to the nature of the ocean medium, the received signal distortion will be different for widely separated sensors in the medium. Consequently, one can expect a certain degree of peak coherence degradation between sensors. When the eigenray signal vectors are widely dispersed over the ambiguity plane, coherence interaction between eigenray correlation pairs will be weak, and the resulting peak intersensor coherence will be equivalent to having received only the strongest of the eigenray signals at each sensor. That is, the presence of the secondary eigenray signals, although increasing the received signal energy at each sensor, contributes little to nothing to the peak cross power (coherence) between sensors. On

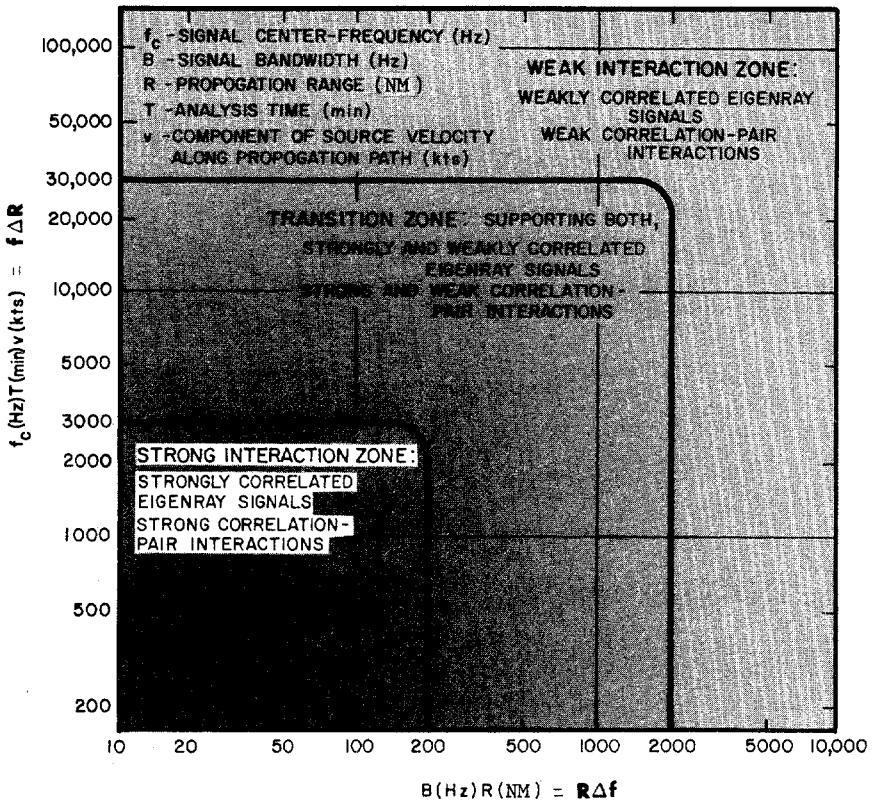

Fig. 12. Map of coherence interaction zones, transformed from the unit circle criteria, for long-range acoustic propagation in the deep ocean. Shading is intended to depict the relative degree of correlation interaction over the graphical area and the fact that the zonal boundaries are somewhat arbitrary.

the other hand, when the eigenray vectors are tightly clustered in the ambiguity plane, the coherence interaction will be strong. Under these circumstances, the peak intersensor coherence (as well as the received signal energy at the sensors) will depend on the relative phases of the ensemble of eigenray signals. The expected peak cross power between sensors will exceed that due to the two primary eigenray signals alone; however, the variance of this cross-power statistic can be quite high. Thus, on the average, the secondary eigenray signals will contribute to intersensor correlation in this case. The coherence interaction zonal map, presented in the last section, provides a convenient means for assessing the efficiency of intersensor correlation in long-range undersea acoustic applications.

Acknowledgment

The author is indebted to his colleagues at the Naval Research Laboratory, particularly, K. D. Flowers, R. M. Fitzgerald, J. D. Shaffer, and A. N. Guthrie, for discussions on the temporal spread of multipath arrivals. Credit is also due to W. L. Anderson for the programming and display of the coherence topologies presented in this paper.

References

[1] A. A. Gerlach, "Acoustic transfer function of the ocean for a motional source," *IEEE Trans. Acoust., Speech, Signal Processing*, vol. ASSP-26, pp. 493-501, Dec. 1978.

[2] R. P. Flanagan, N. L. Weinberg, and J. G. Clark, "Coherent analysis of ray propagation with a moving source and fixed receiver," *J. Acoust. Soc. Amer.*, vol. 56, pp. 1673-1680, Dec. 1974.

[3] G. M. Jacyna and M. J. Jacobson, "Analysis of source-motion effects on sound transmission in the deep ocean," *J. Acoust. Soc. Amer.*, vol. 61, pp. 1153-1162, May 1977.

[4] J. G. Clark and R. P. Flanagan, "Multipath acoustic propagation with a moving source in a bounded ocean channel," *J. Acoust. Soc. Amer.*, vol. 60, pp. 1274-1284, Dec. 1976.

[5] G. M. Jacyna and M. J. Jacobson, "General treatment of source motion on the total acoustic field with application to an isospeed channel," *J. Acoust. Soc. Amer.*, vol. 60, pp. 815-824, Oct. 1976.

[6] J. A. Neubert, "The effect of Doppler on long-range sound propagation," *J. Acoust. Soc. Amer.*, vol. 62, pp. 1404-1411, Dec. 1977.

[7] G. M. Jacyna and M. J. Jacobson, "Deep-water acoustical analysis of stationary and moving broadband sound sources," *J. Acoust. Soc. Amer.*, vol. 63, pp. 1353-1364, May 1978.

[8] K. E. Hawker, "A normal mode theory of acoustic Doppler effects in the oceanic waveguide," *J. Acoust. Soc. Amer.*, vol. 65, pp. 675-681, Mar. 1979.

[9] W. Jobst and X. Zabalgogeazcoa, "Coherence estimates for signals propagated through acoustic channels with multiple paths," *J. Acoust. Soc. Amer.*, vol. 65, pp. 622-630, Mar. 1979.

[10] A. A. Gerlach, *Theory and Applications of Statistical Wave-Period Processing*, vol. 1. New York: Gordon and Breach, 1970, pp. 100-113.

[11] —, "Motion induced coherence degradation in passive systems," *IEEE Trans. Acoust., Speech, Signal Processing*, vol. ASSP-26, pp. 1-15, Feb. 1978.

[12] R. J. Urick, *Principles of Underwater Sound for Engineers.* New York: McGraw-Hill, 1967, pp. 132-135.

[13] Examples of the temporal spread in multipath arrivals as a function of propagation range may be found in D. A. Nutile and A. N. Guthrie, "Propagation paths to Midway Island," *J. Acoust. Soc. Amer.*, vol. 65, pp. 70-74, Jan. 1979.

Albert A. Gerlach received the B.S. degree from the Ohio State University, Columbus, in 1942, the M.S. degree in electrical engineering in 1949, the M.S. degree in mathematics in 1951, and the Ph.D. degree in 1958, all from the Illinois Institute of Technology, Chicago.

He served as a Radar Officer during World War II, and since 1946 he has been engaged in a variety of government-sponsored research and development activities spanning the gamut of electromagnetics, nuclear, aerospace, medical electronics, and underwater acoustics. He has been associated with several commercial firms including the Illinois Institute of Technology Research Institute and the Cook Electric Company. At the latter he served as an Associate Director and Director of Research for the Cook Technology Center Division. Since 1971 he has been with the Acoustics Division, Naval Research Laboratory, Washington, DC, conducting signal processing research in underwater acoustics.

Dr. Gerlach has been active in a number of scientific and professional societies over the past 30 years, serving on a number of technical committees including Chairman of the Chicago Section of the IEEE and founder and Chairman of the Chicago Chapter PGCT. He has published papers in several professional journals covering various areas of circuit theory, signal processing, and underwater acoustics. He is the author of a three-volume book, *Theory and Applications of Statistical Wave-Period Processing*, published by Gordon and Breach in 1970.

Correlator Compensation Requirements for Passive Time-Delay Estimation with Moving Source or Receivers

WILLIAM B. ADAMS, JOHN P. KUHN, AND WILLIAM P. WHYLAND, MEMBER, IEEE

Abstract—**An analysis is given of the effects of source or receiver motions on the output of a cross correlator used to estimate the source time-delay difference across a baseline. For both narrow-band and wide-band correlators, the need for time-varying correlator delay compensation is quantified for the case of a quadratic signal delay-difference variation. Two useful concepts which emerge are 1) the three-dimensional delay/delay-rate/delay-acceleration mean ambiguity function of the source signal, and 2) the equivalent τ-domain filter, which transforms the source autocorrelation function into the mean output of the mismatched correlator.**

The required correlator compensation is approximately a quadratic delay modulation matched to the input delay-difference function. For 3 dB peak output loss with a narrow-band signal, the maximum allowable delay-rate mismatch will produce 158° of phase rotation at the centroid frequency f_0 during the correlation integration time T, while the maximum allowable delay-acceleration mismatch will produce 156° of quadratic phase rotation at f_0 between the center ($t = 0$) and each edge ($t = \pm T/2$) of the correlator integration window. For broad-band signals, the mismatch tolerances become about 11 percent tighter.

I. Introduction

GIVEN two sensors separated by a baseline, passive estimation of the time-delay difference between signals received from a common source may be accomplished by cross correlating the appropriately filtered [1] sensor outputs. When source or receiver motions cause the delay difference to vary, during the correlator integration time T, by more than the correlation time width of the source signal, then the output correlogram is degraded (smeared) unless the correlator implements a compensating delay modulation during T. In many cases the simple expedient of reducing T causes an unacceptable reduction in processing gain.

For a linear delay-difference variation during T, the optimum correlator delay modulation is also linear in time during T, so that one receiver output is time scaled (compressed or expanded) by a constant factor before cross correlating [2]. For a narrow-band signal, this compensation can be approximated by a constant frequency shift [3], [6], [7].

For a quadratic delay-difference variation during T, the optimum correlator delay modulation is approximately quadratic in time during T, so that one receiver output is time scaled by a linearly varying factor before cross correlating. For a narrow-band signal, this compensation can be approximated by a linearly varying frequency shift [3]. If the correlator can only implement a linear delay modulation (or its narrow-band approximation by a constant frequency shift), then the maximum allowable value of T for a specified correlogram degradation becomes a function of the geometry and motion scenario, together with the centroid and width of the source spectrum [3], [4].

All these effects for either broad-band or narrow-band correlators are treated in a unified manner by employing analytic-signal representation, assuming a stochastic source emission,

Manuscript received June 11, 1979; revised October 15, 1979. This work was supported by Naval Systems Command Code 06H1.

The authors are with the Heavy Military Equipment Department, Advanced Development Engineering, Advanced Sonar Concepts, General Electric Company, Syracuse, NY 13221.

0096-3518/80/0400-0158$00.75